



*Conference Proceedings of the 5th Asia Pacific Luminescence and Electron Spin Resonance Dating Conference
October 15th-17th, 2018, Beijing, China*

Guest Editor: Grzegorz Adamiec

THE APPLICATION OF FULL SPECTRUM ANALYSIS TO NaI(Tl) GAMMA SPECTROMETRY FOR THE DETERMINATION OF BURIAL DOSE RATES

MINQIANG BU¹, ANDREW S. MURRAY², MYUNGHO KOOK¹,
JAN-PIETER BUYLAERT^{1,2} and KRISTINA J. THOMSEN¹

¹Center for Nuclear Technologies, Technical University of Denmark, DTU Risø Campus, DK-4000 Roskilde, Denmark

²Nordic Laboratory for Luminescence Dating, Department of Geoscience, Aarhus University, Risø Campus, DK-4000 Roskilde, Denmark

Received 15 February 2019

Accepted 28 October 2019

Abstract: In this study, we explored the potential of a NaI(Tl) scintillator-based gamma spectrometer for the accurate determination of burial dose rates in natural geological samples using a full spectrum analysis (FSA) approach. In this method, an iterative reweighted least-square regression is used to fit calibration standard spectra (⁴⁰K, and ²³⁸U and ²³²Th series in equilibrium) to the sample spectrum, after subtraction of an appropriate background. The resulting minimum detection limits for ⁴⁰K, ²³⁸U, and ²³²Th are 4.8, 0.4 and 0.3 Bq·kg⁻¹, respectively (for a 0.23 kg sample); this is one order of magnitude lower than those obtained with the three-window approach previously reported by us, and well below the concentrations found in most natural sediments. These improved values are also comparable to those from high-resolution HPGe gamma spectrometry. Almost all activity concentrations of ⁴⁰K, ²³⁸U, and ²³²Th from 20 measured natural samples differ by ≤5% from the high resolution spectrometry values; the average ratio of dose rates derived from our NaI(Tl) spectrometer to those from HPGe spectrometry is 0.993 ± 0.004 (n=20). We conclude that our scintillation spectrometry system employing FSA is a useful alternative laboratory method for accurate and precise determination of burial dose rates at a significantly lower cost than high resolution gamma spectrometry.

Keywords: NaI(Tl) detector, scintillation gamma spectrometry, full spectrum analysis (FSA), minimum detection limit (MDL), burial dose rate measurement, OSL dating.

1. INTRODUCTION

In the trapped charge dating community, no matter what techniques and facilities are used, it is important to compare results between different laboratories to show they are all able to measure the same age for the same sample. Such intercomparisons have been well carried out in radiocarbon dating (Scott *et al.*, 2010; Adolphi *et al.*, 2013; Hajdas *et al.* 2017 and Jull *et al.*, 2018), and cosmogenic dating (Vermeesch *et al.*, 2015 and Blard *et al.*, 2015). In luminescence dating, Murray *et al.* (2015) found significant discrepancies in the determination of dose rates in natural samples between more than 20 luminescence dating laboratories using various facilities. These included neutron activation analysis (NAA), inductively-coupled plasma mass spectrometry (ICP-MS), X-ray fluorescence (XRF), atomic absorption spectroscopy (AAS), thick source alpha counting (TSAC), and high resolution gamma spectrometry. Part of this large variability (RSD ~12%) probably arises from the difficulties in homogenising and dissolving samples so that the <500 mg used in, e.g. ICP-MS and NAA is representative. High resolution gamma spectrometry offers an obvious advantage when a more representative and thus usually more accurate dose rate is the aim because it measures samples 100–1000 times larger; a homogenous and representative sample is thus much easier to prepare. However, the high capital cost and level of operator experience required for a reliable operation have hindered its wider application in luminescence dating laboratories.

In a recent preliminary study, Bu *et al.* (2018) showed that a NaI(Tl) scintillator-based gamma spectrometer is also able to determine burial dose rates accurately in natural geological samples, at a significantly lower cost. Using a 3"×3" NaI(Tl) scintillation crystal, they reported minimum detection limits (MDLs) for ^{40}K , ^{238}U , and ^{232}Th activity concentrations of 25, 4.8, and 2.5 $\text{Bq}\cdot\text{kg}^{-1}$, respectively. (MDL is defined here as the activity or activity concentration for which the random uncertainty is 30%, Bu *et al.*, 2018). The above data were obtained using a count time of 20 hours, a 0.19 kg sample and an improved three-window spectrum analysis approach; for 0.23 kg sample used below, these values correspond to 21, 4.0 and 2.1 $\text{Bq}\cdot\text{kg}^{-1}$, respectively. Even though these MDLs are close to or below the lower limits found in most natural sediments, lower MDLs, especially for ^{238}U and ^{232}Th , are desirable to achieve a burial dose rate with lower uncertainty.

In this study, we investigate the potential of a different approach – full spectrum analysis (FSA) (Dean, 1964; Hendriks *et al.*, 2001; Jeong *et al.*, 2014) to reduce the MDLs. An iterative, reweighted least-squares (IRLS) regression (Burrus *et al.*, 1994; Daubechies *et al.*, 2010; Chen *et al.*, 2018) is used to fit three calibration standard spectra (^{40}K , ^{238}U and ^{232}Th series in equilibrium) to the unknown spectrum (after subtraction of an appropriate background). When compared to the three-window ap-

proach, FSA uses considerably more statistical information from each spectrum, and the additional degrees of freedom provide a direct estimate of uncertainties from the fitting process; this is in contrast to the uncertainties in a three-window analysis, which are based only on counting statistics. Here we investigate the benefits of the FSA approach. The revised MDLs are compared with those from both the three-window analysis of Bu *et al.* (2018) and high-resolution HPGe gamma spectrometry (Murray *et al.*, 2018). We also measure 20 representative natural samples and compare the analyses with those from high resolution spectrometry. Finally, we discuss the precision and accuracy available from our NaI(Tl) gamma spectrometer, their dependence on counting time, and the relationship between activity concentration measurement uncertainties and those on dose rates.

2. MATERIALS AND METHODOLOGY

Experimental setup

The configuration of the experimental setup used in this study is essentially the same as the one reported in Bu *et al.* 2018. Briefly, a 3"×3" NaI(Tl) scintillation crystal (Harshaw) and photomultiplier tube (PMT) assembly is connected to a digital tube base (TB-5, Amptek); this contains all necessary electronics for the acquisition of gamma spectra. The entire detector (NaI(Tl) crystal, PMT and digital tube base) is contained within a 10 cm thick lead shield. DppMCA software from Amptek is used to acquire the gamma spectrum. In order to characterise the NaI(Tl) detector, and to evaluate its performance and the accuracy of the algorithm we employ for spectrum analysis (see below), samples were also measured using our standard high resolution HPGe gamma facility (Murray *et al.*, 2018). Because the NaI(Tl) detector and the HPGe detector we used in this study have different dimensions, samples (finely ground sediment mixed with wax and cast in a cup-shape geometry) of different dimensions were prepared for counting on the two different detectors; in each case, these two cups were prepared simultaneously from the same homogenised sediment sample mixture. During data collection, temperatures at the top surface of the NaI(Tl) crystal and in the air in the lead shield were continuously measured by K-type thermocouples and monitored by a thermocouple data logger (USB TC-08, Pico Technology, UK).

Because of atmospheric ^{222}Rn , there can be a correlation between background count rate and atmospheric pressure, season and room ventilation (Mentes and Eper-Pápai, 2015; Schubert *et al.*, 2018). To minimise this effect, we have filled the cavity around the detector with polystyrene foam (Bu *et al.*, 2018); this minimises the volume available to ^{222}Rn contamination. Using this configuration, we have been unable to detect a significant change in background count rate in 6 measurements over a period of 33 weeks.

Sample preparation

All natural samples were ignited at 450°C for 24 hours (to determine organic content) before grinding to <200 µm, and then mixing with high viscosity wax (Bottle wax, blend 1944, British Wax Refining Company) on a hotplate at ~80°C. A typical wax:sample mass ratio of ~1:2 gives a typical sample mass of 250–300 g in the final counting geometry. Sample and calibration standards are cast in the same cup-shaped geometry, with a wall thickness of 10 mm, an internal diameter of 80 mm and an internal height of 60 mm. Samples are stored for >20 days before counting, to allow ^{222}Rn to reach secular equilibrium with its parent ^{226}Ra . Inverted, the sample cups are placed over the top of the NaI detector for counting. Murray *et al.* (2018) report that the dependence of self-attenuation on sample mass for all likely mixtures in the sample cup is <2% over the energy range of interest, *i.e.*, from ~160 keV to ~2.87 MeV.

In order to prepare uranium and thorium calibration standards, the appropriate IAEA certified reference material BL-5 ($7.09 \pm 0.03\%$ U, NRCAN-1) or OKA-2 ($2.893 \pm 0.058\%$ Th, NRCAN-2) was diluted in low activity quartz-rich sand (M32, Sibelco Belgium; ^{226}Ra 1.39 ± 0.08 ; ^{232}Th 0.85 ± 0.06 , ^{40}K $6.8 \pm 0.7 \text{ Bq}\cdot\text{kg}^{-1}$, measured by an HPGe gamma spectrometer), ground to <200 µm. The diluted reference materials were then mixed with wax to give individual parent activities of ~800 Bq per cup. For potassium calibration standards, analytical grade K_2SO_4 ($14.20 \text{ Bq}\cdot\text{g}^{-1}$ assuming stoichiometry, purity given by the manufacturer as 100.4%) was mixed directly with wax to give ~2700 Bq per cup. From the calculation, the expected uncertainties arising from the weighing process are <<1%. Three standards were prepared from separate dilutions for each radionuclide (named as K1-3, U1-3 and Th1-3, respectively). A background sample cup was prepared by casting pure wax. In order to correct for the gain drift caused by temperature changes during counting the algorithm described in Bu *et al.* (2018) employed a common reference spectrum containing all characteristic peaks from ^{40}K , ^{238}U and ^{232}Th . This spectrum was derived from a mixed sample of ^{40}K , ^{238}U and ^{232}Th (named KUTh reference), prepared by diluting BL-5 and OKA-2 in K_2SO_4 to give a sample cup containing ~2700 Bq of ^{40}K and ~70 Bq of ^{238}U and ^{232}Th , respectively. The activity ratios of the three nuclides in this KUTh reference sample are chosen to be similar to the average ratio of ^{40}K , ^{238}U and ^{232}Th activities in natural geological samples (*e.g.*, Ankjærgaard and Murray, 2007 and references therein).

Because our NaI(Tl) scintillation detector is insensitive to low energy photons, photons emitted by ^{222}Rn short-lived daughters dominate the U-series spectrum; given secular equilibrium between ^{222}Rn and ^{226}Ra (ensured by casting in wax and storing), our U analyses are actually ^{226}Ra analyses.

Spectrum drift correction

The full spectrum analysis algorithm used in this study requires considerably more stringent energy stability across the entire spectrum than does the three-window algorithm. After the measurement, spectra from unknown samples, and background and ^{40}K , ^{238}U and ^{232}Th calibration standards were all energy corrected to the common reference spectrum from the KUTh reference sample before spectrum analysis. The linear correction algorithm (with an intercept) corrects two specific peaks in each spectrum to the two corresponding peaks in the reference spectrum. The correction algorithm is described in Bu *et al.* (2018), but we have now improved the selection of the correction reference peaks, especially for correction of ^{40}K calibration standard spectra (in which other peaks are only derived from the background, and so are poorly defined).

The gamma spectra from the background, ^{40}K , ^{238}U and ^{232}Th calibration standards and unknown natural samples all have characteristic peaks of very different absolute and relative intensities; as a result, the most useful reference peaks are dependent on the spectrum to be drift corrected. For example, natural samples usually contain significant activity concentrations of ^{40}K , ^{238}U and ^{232}Th , and so drift correction employs the ubiquitous ~85 keV peak (X-ray) from U and Th, and the 1.46 MeV gamma-ray peak from ^{40}K . The same is true of background spectra although all the intensities are, of course, much weaker. However, this choice is impractical when we select reference peaks for the gamma spectra from calibration standards, *e.g.*, in the ^{40}K standard spectrum, the X-ray peak is not detectable, and so the 1.46 MeV from ^{40}K emission and its Compton backscatter peak (measured at 226 keV) are used. This is in contrast to the more conventional choice of Bu *et al.* (2018), where the 1.46 MeV peak (^{40}K) and the background 2.61 MeV peak from the ^{232}Th series were employed. We now prefer the backscattered peak because the background 2.61 MeV peak is too weak to allow accurate determination of the peak centroid. For the ^{238}U and ^{232}Th calibration standards, we selected the same peaks as those described in Bu *et al.* (2018), *i.e.*, for the ^{238}U calibration standard with negligible ^{40}K , we employ the X-ray peak and the ^{214}Bi peak (1.76 MeV, U series); for ^{232}Th calibration standard, we use the X-ray peak and the ^{208}Tl peak (2.61 MeV).

Fig. 1 illustrates an example of all corrected spectra from one set of ^{40}K , ^{238}U and ^{232}Th calibration standards, a corrected background spectrum, and the KUTh mixed reference spectrum used for drift correction. The shaded region in **Fig. 1** shows the region of interest (ROI) for the full spectrum analysis; this is discussed in more detail in Section 2 – Full spectrum analysis and calculation of activity.

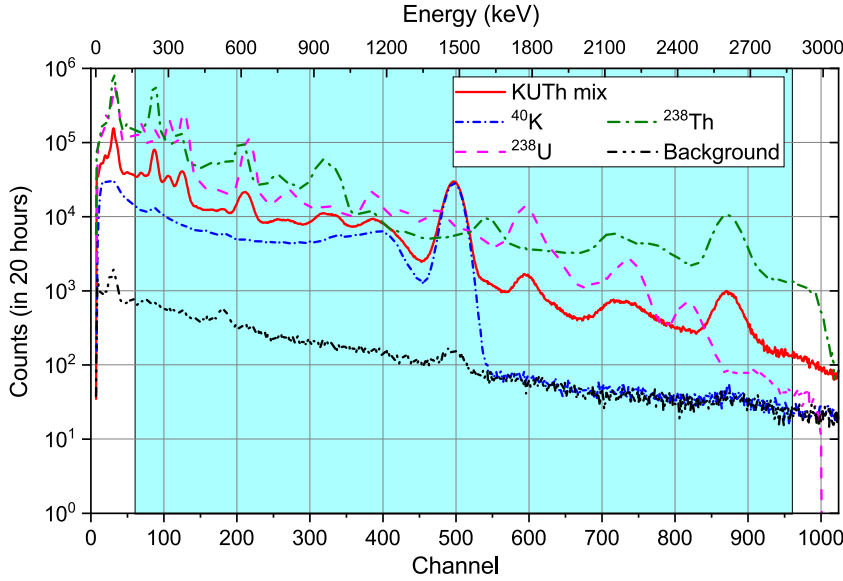


Fig. 1. Drift correction reference spectrum KUTh mix, and drift-corrected spectra from ^{40}K , ^{238}U and ^{232}Th calibration standards and background.

Calibration of detection efficiency

Cups from all three sets of ^{40}K , ^{238}U and ^{232}Th calibration standards (9 in total) were each counted for 20 h, then each spectrum was drift corrected to the reference spectrum, and normalised to counting time to give the count rate in each channel ($\text{counts}\cdot\text{ks}^{-1}$). The background was counted three times (each for 20 h); after correction and normalisation, these three spectra were averaged. This averaged background spectrum was then subtracted from each ^{40}K , ^{238}U and ^{232}Th normalised spectrum. The detection efficiency ($\text{counts}\cdot\text{ks}^{-1}\cdot\text{Bq}^{-1}$) of each nuclide was derived by dividing the count rate in each channel with the known activity (Bq). Finally, the detection efficiencies resulting from three standard spectra were averaged to reduce the contribution to scatter resulting from manufacturing (mainly dilution and casting) of the calibration standards.

Full-spectrum analysis and calculation of activity

In FSA, the shape of a large part of the sample spectrum is analysed, and decomposed to determine the contributions from the three individual ^{40}K , ^{238}U and ^{232}Th standard spectra and the background spectrum. The counts in the first prominent peak (as shown in **Fig. 1**) are mostly X-ray emissions (from U and Th), while the counts above the 2.61 MeV peak are mostly from cosmic rays; these two energy peaks (~ 85 keV and 2.61 MeV) provide limits to the range of energies employed in the FSA. Here, we select a region of interest (ROI) from channel 70 to 960 (in total $M = 891$ channels), corresponding to an energy region from ~ 160 keV to ~ 2.87 MeV.

Formalising the above, in each channel, the measured unknown sample spectrum S is made up of the sum of the ^{40}K , ^{238}U and ^{232}Th detection efficiencies DE_k ($k=1, 2, 3$), each multiplied by the activity A_k contained in the un-

known sample, plus an averaged background spectrum (Bg), *i.e.*:

$$S = \sum_{k=1}^3 DE_k A_k + Bg \quad (2.1)$$

As we know the total number of channels in the energy range of interest is M , in **Eq. 2.1**, there are then M linear equations in total with three unknown variables A_k ($k=1, 2, 3$). We use least-square linear regression to estimate the ^{40}K , ^{238}U and ^{232}Th activities by minimising the chi-squared:

$$\chi^2 = \sum_{i=1}^M [S(i) - \sum_{k=1}^3 DE_k(i) A_k - Bg(i)]^2 \quad (2.2)$$

After obtaining the first estimate of the activities $A_{k,0}$, the estimation accuracy is improved by a second least-squares linear regression following the inclusion of a weight factor $W(i)$ into **Eq. 2.2**:

$$\chi^2 = \sum_{i=1}^M [S(i) - \sum_{k=1}^3 DE_k(i) A_k - Bg(i)]^2 / W(i) \quad (2.3)$$

In **Eq. 2.3**, instead of employing the weight factor $W(i) = S(i)$ as described in Hendriks *et al.* (2001), or as a more complicated form involving estimated activities and uncertainties on all relevant spectra (Jeong *et al.*, 2014), we simply use the absolute value of the fitting error in each channel generated in the previous step as the weight factor $W(i)$.

$$W(i) = |S(i) - \sum_{k=1}^3 DE_k(i) A_{k,0} - Bg(i)| \quad (2.4)$$

In this way, those channels with a higher fitting error have a higher weight factor, giving a faster convergence. We carried out this process iteratively by continuously using a newly obtained $W(i)$ in the current step (defined as step n) as the weight factor for the next step (step $n+1$) of chi-squared minimisation, until the changes in all of the estimated activities reach the condition:

$$|A_{k,n+1} - A_{k,n}| \leq 1e^{-5}Bq \quad (2.5)$$

This process delivers a fitting error contribution of $\sim 0.001 \text{ Bq}\cdot\text{kg}^{-1}$ for a typical $>100 \text{ g}$ sample.

Fig. 2 shows an example using the natural sample (LD791); the original sample spectrum and the fitted spectrum overlap can be seen to agree very well over the entire energy range; the weak structure visible in the residuals presumably arises from errors in the drift corrections.

Uncertainty analysis

The uncertainty analysis on the burial dose rate of natural samples is not a trivial task; there are many sources of uncertainty, both correlated and uncorrelated, contributing to the final propagated uncertainty on the burial dose rate. In this study, as usual, we categorise them into systematic and random uncertainties. The systematic uncertainties depend mainly on the standards we use to calibrate the ^{40}K , ^{238}U and ^{232}Th detection efficiencies on our NaI gamma detector. The random uncertainty includes the uncertainties contributed by the finite counts in each channel (counting statistics) and the fitting uncertainty arising from the fitting algorithm used to determine the activity concentrations. The details of the derivation of systematic and random uncertainties are summarised in the [Supplementary Material](#).

Determination of dose rate

Once the activity concentrations of ^{40}K , ^{238}U and ^{232}Th in the unknown sample are determined, we derive beta and gamma dose rates based on the dose rate conversion factors published by Guérin *et al.* (2011) and Liritzis *et al.* (2013). In addition, we updated various parameters including the atomic weights, abundances and decay constants (and their uncertainties) of ^{40}K , and all U and Th decay series from the IAEA (IAEA Live Chart of

Nuclides, March 2018). The revised activity concentrations per ppm are listed in [Table 1](#). In order to determine the uncertainties in beta and gamma dose rates, updated uncertainties of all relevant quantities, e.g., half-lives, energies, branching ratios, atomic weights, atomic abundances etc., were taken into account and combined during the error propagation process.

During the derivation of field beta and gamma dose rates, radon loss in the field is assumed to be $20\% \pm 10\%$; this is the default assumption used in our laboratory. In addition, we assume ^{226}Ra to be in equilibrium with its series parent ^{238}U . Both these assumptions can be varied on a site-specific basis.

The total dry burial dose rate was then calculated by summing the beta and gamma dose rates. Since the activity concentrations of the ^{238}U and ^{232}Th daughter nuclides are all dependent on activity concentrations of ^{238}U and ^{232}Th , respectively, the contributions from their individual uncertainties to the total beta or gamma uncertainties are correlated. In addition, beta and gamma dose rates are also correlated because they are all derived from the same ^{40}K , ^{238}U and ^{232}Th activity concentrations. During the summing of beta and gamma dose rates, propagation of these correlated uncertainties are handled by the uncertainty analysis tool *Metas.UncLib* (Zeier *et al.*, 2012), in the same manner as the uncertainties for the activities (see [Supplementary Material](#)).

Table 1. Updated ^{40}K , ^{238}U and ^{232}Th activity concentration per ppm for dose rate derivation.

Radionuclide	Activity concentration ($\text{Bq}\cdot\text{kg}^{-1}$)	Uncertainty ($\text{Bq}\cdot\text{kg}^{-1}$)
^{40}K	317	3
^{238}U	12.922	0.025
^{232}Th	4.061	0.029

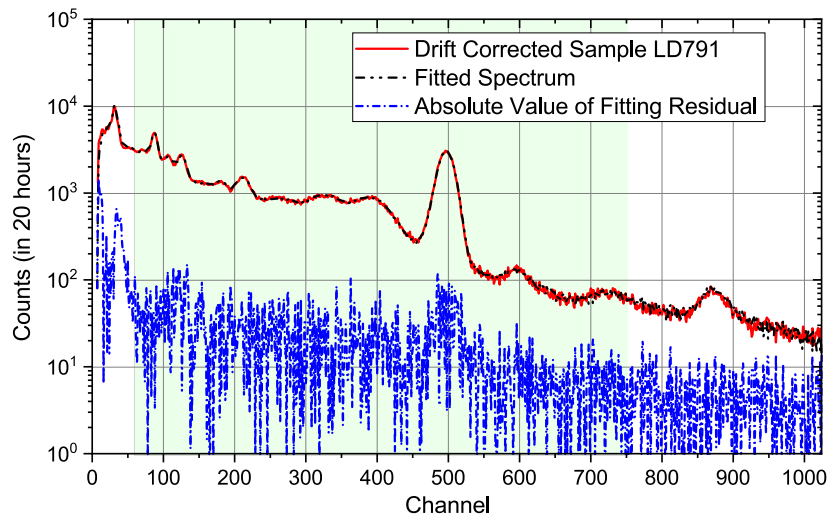


Fig. 2. Illustration of the agreement of a calculated fitted spectrum with the original sample spectrum, together with fitting residuals in each channel.

3. RESULTS AND DISCUSSION

Minimum detection limits (MDLs)

MDLs for ^{40}K , ^{238}U and ^{232}Th activities (or activity concentrations for a sample with a certain weight) are one of the most important specifications of a gamma spectrometer intended for the measurement of dose rates. In this study, we used the same procedures as described in Bu *et al.* (2018) to measure these MDLs experimentally. In short, we measured the same KUTh mixed sample cup for ten various lengths of time t : 30, 60, 120, 300, 600, 1200, 2400, 4500, 9000 and 72000 s. The background cup was counted for 72000, 71970, 71940, 71880, 71700, 71400, 70800, 69600, 67500, 63000 s. After drift correction, we combine a sample spectrum (e.g. that counted for 30 s) with the corresponding background spectrum (in this case, that counted for 71970 s) to give a spectrum corresponding to a total effective counting time of 72000 s (20 hours). This gives us in total ten synthesised spectra equivalent to those that would have been obtained from ten samples of well-known relative activity concentrations; all counted for 20 h. The expected activity concentration (A_{EXP}) corresponding to the counting time t of

each synthesised sample was calculated from the activity concentration measured for 20 h (A_{MEAS_20h}):

$$A_{EXP} = A_{MEAS_20h} \times t/72000 \quad (3.1)$$

These ten synthesised sample spectra were analysed by FSA and the apparent ^{40}K , ^{238}U and ^{232}Th activities (A_{MEAS}) derived. Here we define the MDL as the value of A_{EXP} expected to have a corresponding random uncertainty of 30% on A_{MEAS} . Fig. 3a–3c summarises the FSA analysis results, and gives MDLs for ^{40}K , ^{238}U and ^{232}Th activities of 1.1, 0.09 and 0.07 Bq, respectively. By dividing by the maximum practical sample mass in our cup geometry (0.23 kg), the corresponding MDLs on activity concentrations for ^{40}K , ^{238}U and ^{232}Th are 4.8, 0.4 and 0.3 Bq·kg⁻¹, respectively. Table 2 compares these FSA MDLs with those from the three-window approach (Bu *et al.*, 2018) from a NaI(Tl) spectrometer, and MDLs from a high resolution HPGe gamma spectrometer (Murray *et al.*, 2018). Table 2 shows FSA MDLs are one order of magnitude lower than those achieved by three-window spectrum analysis, and are one order of magnitude higher than those from an HPGe detector. This indicates the FSA approach is a significant improvement on the results

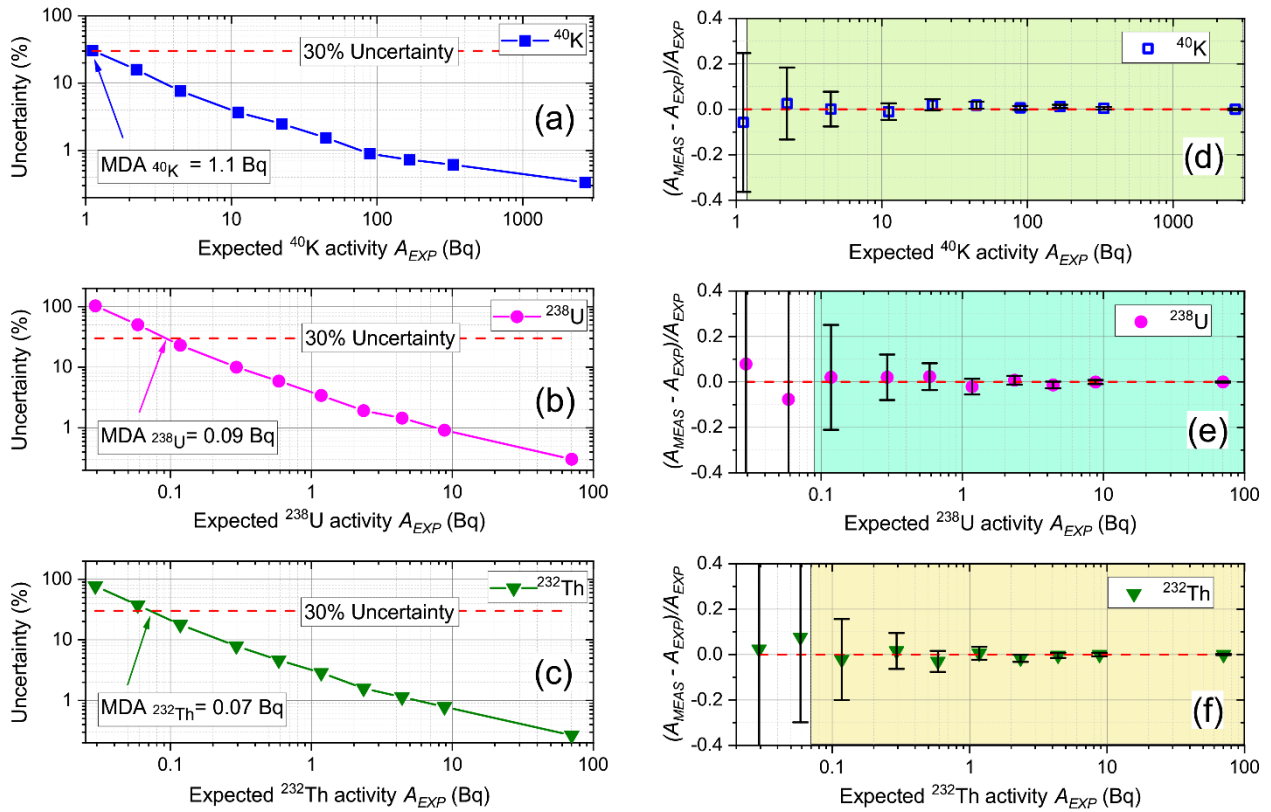


Fig. 3. (a–c) Minimum detection limits (MDLs) for activities of ^{40}K , ^{238}U and ^{232}Th , respectively, defined as random uncertainty approaching 30%, when random uncertainty is expressed as a function of expected activity (A_{EXP}); (d–f) Comparison of measured ^{40}K , ^{238}U and ^{232}Th activity concentration (A_{MEAS}) and expected activity concentration (A_{EXP}), showing the accuracy of measurement and FSA analysis. The error bars in panels (d–f) shows the random uncertainty.

Table 2. Comparison of MDLs ($Bq \cdot kg^{-1}$) from different studies.

Nuclide	NaI(Tl) spectrometer (Sample weight: 0.23 kg)		HPGe spectrometer (Sample weight: 0.25 kg) (Murray <i>et al.</i> , 2018)
	FSA (This study)	3-Window (Bu <i>et al.</i> , 2018)	
^{40}K	4.8	21	0.6
^{238}U	0.4	4.0	0.04
^{232}Th	0.3	2.1	0.03

obtainable from a low resolution NaI(Tl) gamma spectrometer, presumably because of much greater statistical precision. The total number of counts recorded in the energy region of interest in FSA is orders of magnitude greater than that in the windows-of-interest in the three-window approach; the FSA approach makes use of almost all statistical information contained in the sample spectrum.

Measurement accuracy and precision

The accuracy of the measurement and analyses can be examined in **Fig. 3d–3f**, in which the shaded regions in all three subpanels represent the activity ranges above MDLs, for ^{40}K , ^{238}U and ^{232}Th , respectively. The deviations $A_{MEAS} - A_{EXP}$ between the measured and expected activities for ^{40}K , ^{238}U and ^{232}Th , are normalised to the expected activity A_{EXP} , as shown in **Fig. 3d–3f**, as a function of A_{EXP} . The error bars shown in **Fig. 3d–3f** are derived from the random uncertainties of the expected and measured activities. Within these shaded regions, ^{40}K , ^{238}U , and ^{232}Th analyses are all consistent with the expected results, without any obvious systematic error, even when the expected activities approach the MDLs.

The precision and accuracy of the FSA algorithm were further evaluated by comparison of our analyses with those from a high resolution HPGe spectrometry facility (Murray *et al.*, 2018; making the same assumptions concerning secular equilibrium), using 20 natural samples covering a range of activity concentrations. **Fig. 4a–4c** shows the deviation $AC_{NaI} - AC_{HPGe}$ between activity concentrations obtained from the NaI(Tl) spectrometer and those from the HPGe spectrometer are normalised to AC_{HPGe} . The resulting dry dose rates for all 20 unknown samples are normalised in the same manner, and the normalised deviations are compared in **Fig. 4d**.

In this study, all unknown samples, ^{40}K , ^{238}U and ^{232}Th calibration standard cups, mixed KUTh reference cup for drift correction and background cup were measured at a room temperature of ~ 20 – $25^\circ C$ for 20 hours. The maximum temperature drift during each measurement was $\sim 0.4^\circ C$.

As shown in **Fig. 4a–4c**, almost all normalised deviations $(AC_{NaI} - AC_{HPGe})/AC_{HPGe}$ of ^{40}K , ^{238}U and ^{232}Th for 20 samples lie within the shaded region of $\pm 5\%$, with only one data point below -5% line in ^{238}U panel and another two just above $+5\%$ line in ^{232}Th panel. For the total beta and gamma dose rates (**Fig. 4d**), normalised deviations $(DR_{NaI} - DR_{HPGe})/DR_{HPGe}$ lie within the shaded region ($\pm 4\%$) for all 20 studied samples. The standard deviations ($n=20$) on these ratios are also listed in each subpanel in **Fig. 4**. All activity concentration ratios have a standard deviation of $< 3\%$, and the corresponding variability in dose rates is $< 2\%$.

In addition, **Fig. 4a–4d** show that there is no suggestion of a systematic deviation, either in the activity concentrations or in the total dry beta and gamma dose rates.

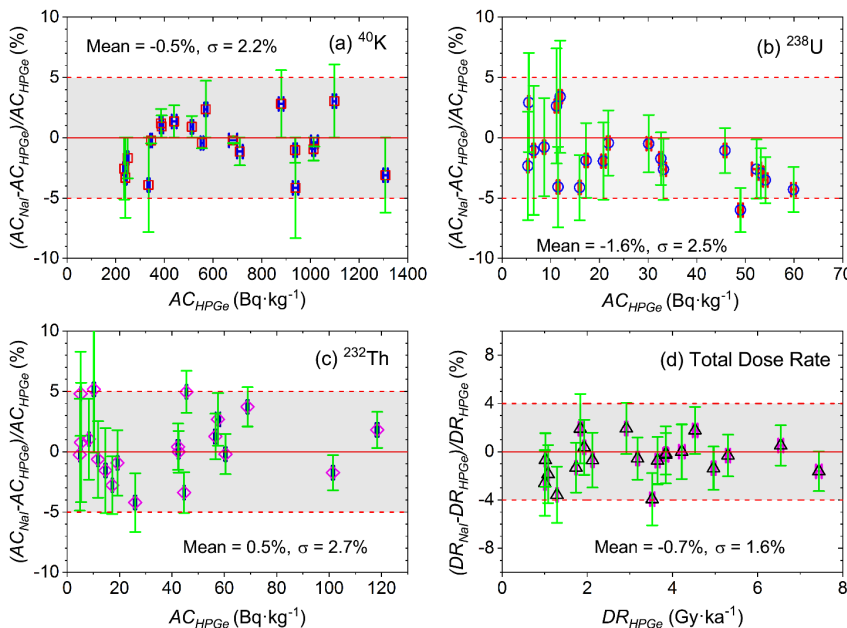


Fig. 4. Normalized deviations between those activity concentrations for ^{40}K , ^{238}U and ^{232}Th (a–c), and total ($\beta + \gamma$) dose rates (d) determined by the NaI(Tl) spectrometer and those determined by an HPGe spectrometer, for 20 geological samples. The shaded regions represent $\pm 5\%$ deviation in panels (a–c), and $\pm 4\%$ deviation in panel (d). The standard deviation for 20 data in each subpanel show a high measurement precision on NaI(Tl) spectrometer. All error bars in panel (a–c) and in panel (d) are derived from the total uncertainties of AC_{NaI} and AC_{HPGe} , and total uncertainties of DR_{NaI} and DR_{HPGe} , respectively.

This is also indicated in **Table 3** by the average ratios of AC_{NaI}/AC_{HPGe} and DR_{NaI}/DR_{HPGe} , with low standard deviations ($n = 20$) of 0.4 to 0.6%.

Table 3. Average ratios of AC_{NaI}/AC_{HPGe} and DR_{NaI}/DR_{HPGe} ($n = 20$).

	Average ratio
^{40}K	0.995 ± 0.005
^{238}U	0.984 ± 0.005
^{232}Th	1.005 ± 0.006
Total dose rate	0.993 ± 0.004

Counting time

Another important consideration when using a gamma spectrometer for measuring dose rates in OSL dating applications is the counting time. The required count time is dictated by the required dose rate uncertainty and the sample activity. As discussed above, the total uncertainty on dose rate is mainly derived from random and systematic uncertainty in ^{40}K , ^{238}U and ^{232}Th activity concentrations. While the systematic uncertainty is fixed (at $\sim 2\%$), the random uncertainty, no matter whether from the fitting error of FSA algorithm or from counting statistics, is mainly determined by the counts in each channel.

Quantitative investigation of the dependency on counting time was carried out by counting the same natural sample (LD962) for different lengths of time, *i.e.*, 5, 10, 20, 30 min, and 1, 2, 5, 10, 20 hours. **Fig. 5a–5c** and (d) show the dependence of the measured activity con-

centrations of ^{40}K , ^{238}U and ^{232}Th , and total beta and gamma dose rates, respectively, on counting time. The results are compared with those measured on the HPGe spectrometer for 20 hours, *i.e.*, 235, 8.6, and 8.3 Bq·kg⁻¹ for activity concentrations of ^{40}K , ^{238}U and ^{232}Th and 1.09 Gy·ka⁻¹ for total dose rate; these values are represented by the thick horizontal dashed lines in each sub-panel in **Fig. 5**. The shaded region in each subpanel links to the right vertical axis and shows the dependence of the corresponding normalised deviations between the results from the NaI(Tl) spectrometer and the HPGe spectrometer for activity concentrations $(AC_{NaI} - AC_{HPGe})/AC_{HPGe}$ (**Fig. 5a–5c**) and for corresponding derived dose rates $(DR_{NaI} - DR_{HPGe})/DR_{HPGe}$ (**Fig. 5d**). These data indicate the counting times required to achieve a specified level of precision in the activity concentrations of ^{40}K , ^{238}U and ^{232}Th and the derived dose rate, e.g. a 30 min count will lead to a $\sim \pm 10\%$ uncertainty on dose rate.

Fig. 6 shows the variation in the uncertainty on the total dose rate with the counting time, for a sample with 235, 8.6, and 8.3 Bq·kg⁻¹ of ^{40}K , ^{238}U and ^{232}Th , respectively and a dose rate of 1.09 Gy·ka⁻¹. These data allow the selection of the count time required to achieve a specified uncertainty. For example, even counting for only 1 to 2 hours gives a dose rate with a relative uncertainty $\leq 5\%$. A longer count of > 5 hours brings down the uncertainty below $\pm 3\%$. The sample used to illustrate these dependencies is amongst those with the lowest activity concentrations (see **Fig. 4**); one can expect to obtain even lower uncertainties with a shorter counting time when the samples with higher activity concentrations are measured.

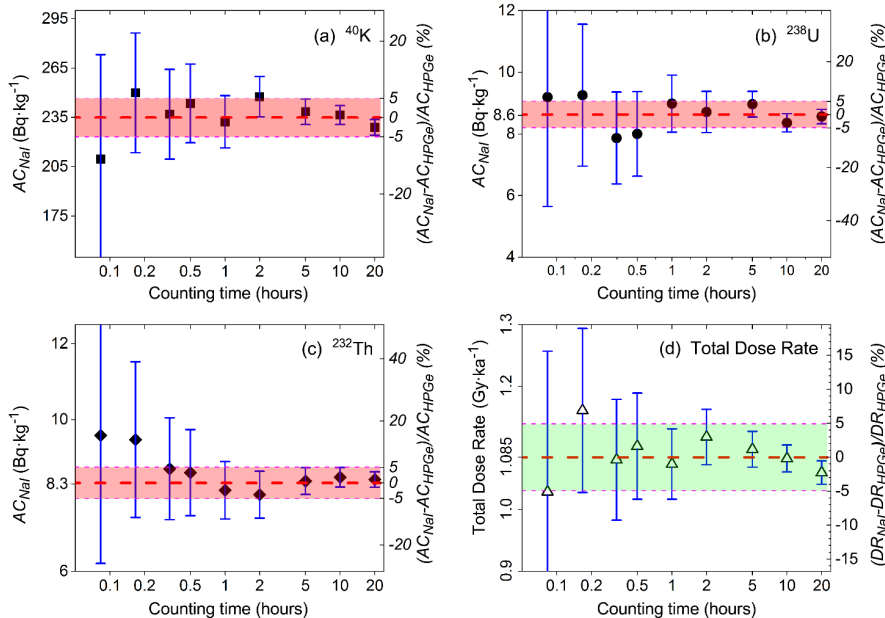


Fig. 5. Activity concentrations (a-c) and total dose rate (d) of a natural sample (LD962) counted with different counting time on NaI(Tl) spectrometer. The horizontal dashed line in the centre of shaded region in each subpanel represents the activity concentration (a-c) and total dose rate (d) from HPGe spectrometer. All error bars in panel (a-c) and in panel (d) denote the total uncertainties of AC_{NaI} , and total uncertainties of DR_{NaI} , respectively.

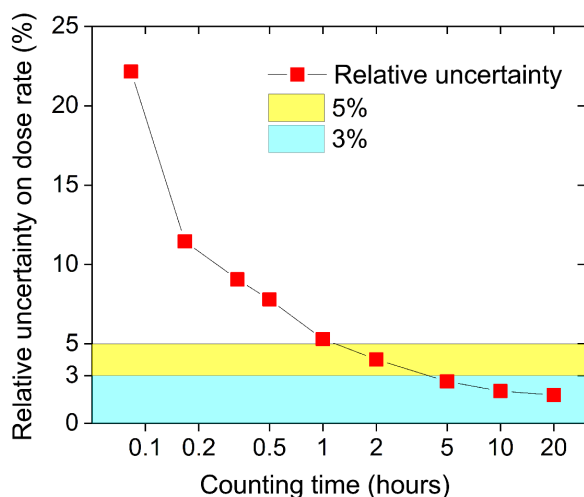


Fig. 6. Dependence of relative total dose rate uncertainty on counting time, for a sample containing 235, 8.6, and 8.3 Bq·kg⁻¹ of ⁴⁰K, ²³⁸U and ²³²Th, respectively and a total dose rate of 1.09 Gy·ka⁻¹.

4. CONCLUSIONS

We have investigated the potential of full spectrum analysis (FSA) algorithm for analysing gamma spectra from a low cost, low maintenance laboratory spectrometry system based on a 3''×3'' NaI(Tl) crystal, to determine burial dose rates in trapped charge dating. Experimental results have shown that an FSA algorithm employing iterative reweighted least-squares regression is able to significantly lower the minimum detection limits (MDLs), down to 1.1, 0.09, and 0.07 Bq, respectively, for ⁴⁰K, ²³⁸U, and ²³²Th activities (corresponding to 4.8, 0.4 and 0.3 Bq·kg⁻¹ for a 0.23 kg sample). These MDLs are one order of magnitude lower than those based on an improved three-window analysis approach (reported earlier by Bu *et al.*, 2018), and are comparable to those obtained from our high resolution HPGe facility (Murray *et al.*, 2018). The MDLs for ⁴⁰K, ²³⁸U, and ²³²Th from FSA are all almost one order of magnitude lower than those found in almost all natural sediments. We conclude that our NaI(Tl) gamma analyses based on FSA are suitable for determining the dose rate even in samples containing low activity concentrations of ⁴⁰K, ²³⁸U and ²³²Th.

The accuracy and precision on measurement and analysis of activity concentration and dose rate have been examined in 20 natural samples. The results are also compared to those measured using an HPGe spectrometer, and we found the relative discrepancies are all within 5% on activity concentrations of ⁴⁰K (RSD 2.2%), ²³⁸U (RSD 2.5%), and ²³²Th (RSD 2.7%), and within 4% on dose rates (RSD 1.6%). The average ratio of dose rates measured on our NaI(Tl) scintillation spectrometer with FSA to those from HPGe spectrometry is 0.993 ± 0.004 (n=20).

Further investigations of the dependence of analyses on counting time indicate that for a sample containing ~250, 10 and 10 Bq·kg⁻¹ of ⁴⁰K, ²³⁸U and ²³²Th, respectively, even a 1–2 hours count time gives a result with uncertainty ≤5%. A longer counting, e.g. for 5 hours quickly brings down the uncertainty below ±3%. This demonstrates that using FSA with our NaI(Tl) spectrometer is capable of rapid and accurate determination of burial dose rate.

Given these results, we conclude that our simple scintillation spectrometry system employing FSA is a useful alternative laboratory method for accurate and precise determination of burial dose rates at a significantly lower cost than high resolution gamma spectrometry. This, combined with the relatively large (and so more representative) sample size, makes it a strong competitor to other analytical methods used in OSL dating.

SUPPLEMENTARY MATERIAL

Supplementary material is available online at <http://dx.doi.org/10.2478/geochr-2020-0009>. Here we provide detailed information on how we derive the systematic and random uncertainties, and how these are summed to give total uncertainties on ⁴⁰K, ²³⁸U and ²³²Th activities.

ACKNOWLEDGEMENTS

J.-P. Buylaert received funding from the European Research Council under the European Union Horizon 2020 research and innovation programme (grant number: ERC-2014-StG 639904 – RELOS).

REFERENCES

- Adolphi F, Gütler D, Wacker L, Skog G and Muscheler R, 2013. Intercomparison of C-14 dating of wood samples at Lund University and ETH Zurich AMS facilities: extraction, graphitization, and measurement. *Radiocarbon* 55(2–3): 391–400, DOI 10.1017/S0033822200057519.
- Ankjaergaard C and Murray AS, 2007. Total beta and gamma dose rates in trapped charge dating based on beta counting. *Radiation Measurements* 42: 352–359, DOI 10.1016/j.radmeas.2006.12.007.
- Blard PH, Balco G, Burnard PG, Farley KA, Fenton CR, Friedrich R, Jull AJT, Niedermann S, Pik R, Schaefer JM, Scott EM, Shuster DL, Stuart FM, Stute M, Tibari B, Winckler G and Zimmermann L, 2015. An inter-laboratory comparison of cosmogenic ³He and radiogenic ⁴He in the CRONUS-P pyroxene standard. *Quaternary Geochronology* 26: 11–19, DOI 10.1016/j.quageo.2014.08.004.
- Bu M, Murray AS, Kook M, Helsted LM, Buylaert J-P and Thomsen KJ, 2018. Characterisation of scintillator-based gamma spectrometers for determination of sample dose rate in OSL dating applications. *Radiation Measurements* 120: 253–259, DOI 10.1016/j.radmeas.2018.07.003.
- Burrus CS, Barreto JA and Selesnick IW, 1994. Iterative reweighted least squares design of FIR filters. *IEEE Transactions on Signal Processing* 42(11): 2926–2936, DOI 10.1109/78.330353.
- Chen C, He L, Li H and Huang J, 2018. Fast iteratively reweighted least squares algorithms for analysis-based sparse reconstruction. *Medical Image Analysis* 49: 141–152, DOI 10.1016/j.media.2018.08.002.

- Daubechies I, DeVore R, Fornasier M and Gunturk CS, 2010. Iteratively reweighted least squares minimization for sparse recovery. *Communications on Pure and Applied Mathematics* 63(1):1–38, DOI 10.1002/cpa.20303.
- Dean P, 1964. Computer Techniques in γ spectrometry. In: Adams J and Lowder W, eds., *The Natural Radiation Environment*. The University of Chicago Press, pp.617–626.
- Guérin G, Mercier N and Adamiec G, 2011. Dose-rate conversion factors: Update. *Ancient TL* 29: 5–8.
- Hajdas I, Lindroos A, Heinemeier J, Ringbom A, Marzaioli F, Terrasi F, Passariello I, Capano M, Artioli G, Addis A, Secco M, Michalska D, Czernik J, Goslar T, Hayen R, Van Strydonck M, Fontaine L, Boudin M, Maspero F, Panzeri L, Galli A, Urbanova P and Guibert P, 2017. Preparation and dating of mortar samples-mortar dating inter-comparison study (MODIS). *Radiocarbon* 59(6):1845–1858, DOI 10.1017/RDC.2017.112.
- Hendriks PHGM, Limburg J and de Meijer RJ, 2001. Full-spectrum analysis of natural γ -ray spectra. *Journal of Environmental Radioactivity* 53: 365–380, DOI 10.1016/S0265-931X(00)00142-9.
- IAEA Live Chart of Nuclides, March 2018. nuclear structure and decay data, WEB site: <<https://www-nds.iaea.org/relnsd/vcharthtml/VChartHTML.html>>. Accessed 2018.10.10.
- Jeong M, Lee KB, Kim KJ, Lee M-K and Han J-B, 2014. Gamma-ray Full Spectrum Analysis for Environmental Radioactivity by HPGe Detector. *Journal of Astronomy and Space Science* 31(4): 317–323, DOI 10.5140/JASS.2014.31.4.317.
- Jull AJT, Pearson CL, Taylor RE, Southon JR, Santos GM, Kohl CP, Hajdas I, Molnar M, Baisan C, Lange TE, Cruz R, Janovics R and Major I, 2018. Radiocarbon Dating and Intercomparison of Some Early Historical Radiocarbon Samples. *Radiocarbon* 60(2): 535–548, DOI 10.1017/RDC.2018.18.
- Liritzis I, Stamoulis K, Papachristodoulou C and Ioannides K, 2013. A re-evaluation of radiation dose-rate conversion factors. *Mediterranean Archaeology and Archaeometry* 13(3): 1–15.
- Mentes G and Eper-Pápai I, 2015. Investigation of temperature and barometric pressure variation effects on radon concentration in the Sopronbánfalva Geodynamic Observatory, Hungary. *Journal of Environmental Radioactivity* 149: 64–72, DOI 10.1016/j.jenvrad.2015.07.015.
- Murray AS, Buylaert J-P and Thiel C, 2015. A luminescence dating intercomparison based on a Danish beach-ridge sand. *Radiation Measurements* 81: 32–38, DOI 10.1016/j.radmeas.2015.02.012.
- Murray AS, Helsted LM, Autzen M, Jain M and Buylaert J-P, 2018. Measurement of natural radioactivity: calibration and performance of a high-resolution gamma spectrometry facility. *Radiation Measurements* 120: 215–220, DOI 10.1016/j.radmeas.2018.04.006.
- NRCAN-1, Uranium Ore BL-5, Natural Resources Canada, WEB: <<http://www.nrcan.gc.ca/mining-materials/certified-reference-materials/certificate-price-list/8115>>.
- NRCAN-2, Thorium Ore OKA-2, Natural Resources Canada, WEB: <<http://www.nrcan.gc.ca/mining-materials/certified-reference-materials/certificate-price-list/8135>>.
- Scott E, Cook G and Naysmit P, 2010. The fifth international radiocarbon intercomparison (VIRI): an assessment of laboratory performance in stage 3. *Radiocarbon* 53(2–3): 859–865, DOI 10.1017/S003382220004594X.
- Schubert M, Musolff A and Weiss H, 2018. Influences of meteorological parameters on indoor radon concentrations (^{222}Rn) excluding the effects of forced ventilation and radon exhalation from soil and building materials. *Journal of Environmental Radioactivity* 192: 81–85, DOI 10.1016/j.jenvrad.2018.06.011.
- Vermeesch P, Balco G, Blard PH, Dunai TJ, Kober F, Niedermann S, Shuster DL, Strasky S, Stuart FM, Wieler R and Zimmermann L, 2015. Interlaboratory comparison of ^{21}Ne in quartz. *Quaternary Geochronology* 26: 20–28, DOI 10.1016/j.quageo.2012.11.009.
- Zeier M, Hoffmann J and Wollensack M, 2012. Metas.UncLib—a measurement uncertainty calculator for advanced problems. *Metrologia* 49: 809–815, DOI 10.1088/0026-1394/49/6/809.